RSC Advances

PAPER

View Article Online
View Journal | View Issue

Check for updates

Cite this: *RSC Adv.*, 2025, **15**, 2242

Aggregation-induced emission in novel multilayered 3D polymers: development of a fluorescent probe for selective metal ion detection†

Sai Zhang, *[a] Qingkai Yuan,[b] Qingzheng Xu,[c] Shenghu Yan,[a] Yue Zhang*[a] and Guigen Li *[b]

This study presents the characterization of a novel multilayered three-dimensional (3D) polymer exhibiting aggregation-induced emission (AIE) properties when excited at a low wavelength of 280 nm. Utilizing fluorescence spectroscopy, we demonstrate that the polymer displays a marked enhancement in luminescence upon aggregation, a characteristic behavior that distinguishes AIE-active materials from conventional fluorophores. Furthermore, we explore the potential application of this multilayered 3D polymer as a fluorescent probe for the selective detection of specified metal ions. By incorporating chelating functional groups into the polymer matrix, we facilitate specific interactions with target metal ions, leading to significant fluorescence intensity changes that correlate with ion concentration. According to their cyclic voltammetry characteristics, the polymers have potential applications in cutting-edge electrical and optoelectronic systems. Our findings indicate that this multilayered 3D polymer serves as an effective fluorescent sensor and offers tunable optical properties, paving the way for innovative applications in environmental monitoring and biomedical diagnostics. The results underscore the utility of AIE-active polymers in developing advanced materials for sensitive and selective detection of metal ions, contributing to the growing field of smart sensing technologies.

Received 4th December 2024
Accepted 21st December 2024

DOI: 10.1039/d4ra08548e

rsc.li/rsc-advances

Open Access Article. Published on 23 January 2025. Downloaded on 2/12/2026 10:28:10 AM.
This article is licensed under a Creative Commons Attribution-NonCommercial 3.0 Unported Licence.

1 Introduction

The quest for advanced materials with enhanced optical properties has become a focal point of research in polymer science, particularly in the context of photonic applications.[1–8] Among the various classes of materials, multilayered three-dimensional (3D) polymers stand out due to their unique structural configurations and tunable properties.[9–12] These polymers can be designed to exhibit a wide range of functionalities, making them suitable for applications in sensors,[13] drug delivery systems,[14–16] and imaging technologies.[17,18] Their structural intricacies allow for the manipulation of molecular interactions, which can significantly influence their optical behaviors.

A particularly intriguing phenomenon associated with certain organic materials is aggregation-induced emission (AIE).[19–21] Unlike conventional fluorophores, which often experience a reduction in luminescence upon aggregation due to concentration quenching, AIE-active materials exhibit enhanced fluorescence in aggregated states. This counterintuitive behavior is attributed to the restriction of intramolecular motions that typically dissipate energy as heat in non-aggregated states. The AIE phenomenon has opened new avenues for the design of efficient fluorescent probes,[22] which are essential for various analytical applications,[23] including environmental monitoring,[24] biomedical imaging,[25] and sensing of metal ions[26] and specified functional group.[27]

The detection of metal ions is of paramount importance across multiple disciplines, including environmental science, biochemistry, and materials science.[28] Metal ions play critical roles in biological systems, yet their excessive accumulation can lead to toxicological effects. Therefore, the development of sensitive and selective fluorescent probes for the detection of specific metal ions is essential. Traditional methods for metal ion detection, such as atomic absorption spectroscopy and inductively coupled plasma mass spectrometry, are often expensive and require sophisticated instrumentation. In contrast, fluorescence-based sensors offer distinct advantages, including high sensitivity, rapid response times, and the potential for real-time monitoring.

[a]School of Pharmacy, Continuous Flow Engineering Laboratory of National Petroleum and Chemical Industry, Changzhou University, Changzhou, Jiangsu 213164, China
[b]Department of Chemistry, Texas Tech University, Lubbock, TX 79415, USA
[c]School of Chemistry and Chemical Engineering, Nanjing University, Nanjing, Jiangsu, 210093, China

† Electronic supplementary information (ESI) available. See DOI: https://doi.org/10.1039/d4ra08548e

© 2025 The Author(s). Published by the Royal Society of Chemistry

Open Access Article. Published on 23 January 2025. Downloaded on 2/12/2026 10:28:10 AM.
This article is licensed under a Creative Commons Attribution-NonCommercial 3.0 Unported Licence.

In this study, we report on the characterization of a novel multilayered 3D polymer that exhibits AIE properties when excited at low wavelengths, specifically 280 nm. Utilizing fluorescence spectroscopy, we demonstrate the polymer's ability to emit strong fluorescence in an aggregated state, confirming the presence of the AIE phenomenon. Furthermore, we explore the potential of this multilayered 3D polymer as a fluorescent probe for the selective detection of specified metal ions.

The synthesis of the multilayered 3D polymer involves a carefully controlled polymerization process that allows for the precise arrangement of functional groups within the polymer matrix.[9–12] This structural design is pivotal for enhancing the polymer's interaction with target metal ions. By incorporating specific chelating groups into the polymer backbone, we aim to achieve selective binding with metal ions, thereby facilitating their detection through fluorescence signaling. To evaluate the fluorescence response of the synthesized polymer in the presence of various metal ions, we conducted a series of experiments that involved exposing the polymer to solutions containing different concentrations of target ions. The resulting fluorescence intensity was measured and correlated with the concentration of the metal ions, allowing us to establish a calibration curve for quantitative analysis. Our findings indicate that the multilayered 3D polymer exhibits a marked increase in fluorescence intensity upon binding with specific metal ions, confirming its potential as a reliable fluorescent probe.[29–35]

The advantages of using a multilayered 3D polymer as a fluorescent probe extend beyond mere sensitivity. The structural complexity of the polymer enables a high degree of tunability, allowing for the optimization of its optical properties based on the specific requirements of the application. Moreover, multilayered architecture enhances the stability and reproducibility of the sensor, which are critical factors for practical applications in real-world scenarios. In addition to its application as a fluorescent probe for metal ion detection, the multilayered 3D polymer holds promise for a range of other applications. Its unique optical properties and structural versatility can be harnessed in the development of biosensors, where the polymer could be functionalized to detect biomolecules such as proteins or nucleic acids. Furthermore, the ability to tailor the polymer's properties through copolymerization or post-synthesis modifications opens up new avenues for research and development in the field of smart materials.

In this research, we present a comprehensive investigation into the synthesis and characterization of a multilayered 3D polymer that exhibits AIE properties upon excitation at 280 nm. The polymer's potential as a fluorescent probe for the selective detection of specified metal ions has been demonstrated, highlighting its applicability in various analytical contexts. The findings contribute to the growing body of knowledge surrounding AIE-active materials and their integration into advanced polymeric systems, paving the way for innovative applications in environmental monitoring, biomedical diagnostics, and beyond. Future work will focus on further optimizing the polymer's properties and exploring its capabilities in complex matrices, thereby enhancing its utility as a versatile tool in the detection of metal ions and other analytes.

2 Experimental section

All synthetic procedures of polymer **1** and **2** (Fig. 1) have been published in the former work.[12] Photoluminescence spectra were obtained using Shanghai Lengguang F98, UV-Vis absorption spectra were measured with Shanghai Lengguang 759s. Cyclic voltammetry was measured by DH Instrument 7000D electrochemical analyzer with a three-electrode cell, Ag/AgCl referenced against ferrocene/ferrocenium (Fc/Fc^+), 0.10 eV and platinum wire as the counter electrode.

3 Results and discussions

3.1 Ultraviolet (UV) spectroscopy

Ultraviolet (UV) spectroscopy is a powerful analytical technique that plays a crucial role in the characterization of multilayered 3D polymers. Ultraviolet (UV) spectroscopy can provide insights into the interactions between different polymer layers. Changes in the absorption spectra upon layering can indicate physical or chemical interactions, such as hydrogen bonding or charge transfer, which can significantly affect the material properties and performance. During the fabrication of multilayered polymers, ultraviolet (UV) spectroscopy can be used to monitor the progress of polymerization and crosslinking reactions. This real-time analysis helps in optimizing processing conditions to achieve desired mechanical and thermal properties.

We discovered an extremely evident "tailing phenomenon" in the different water fractions when we investigated the ultraviolet (UV) spectroscopy of polymers **1** and **2** (Fig. 2). When the water fraction was raised from 0% to 70% at the same concentration, polymer **1**'s "tailing phenomenon" was less evident than polymer **2**'s. The tailing phenomenon often indicates the presence of aggregated species, which can arise from intermolecular interactions that promote the formation of larger, non-covalent assemblies. In the context of thiophene-based polymers, these interactions could be facilitated by π–π stacking or hydrophobic interactions among the polymer chains. Such aggregation can lead to altered electronic properties, manifesting as spectral anomalies in the UV region. Furthermore, the chiral nature of the polymer could enhance these interactions, resulting in a more pronounced aggregation tendency. This aggregation-induced effect could significantly influence the optical behavior of the material, potentially affecting its chiroptical properties and overall performance in applications such as sensors or photonic devices. Thus, the

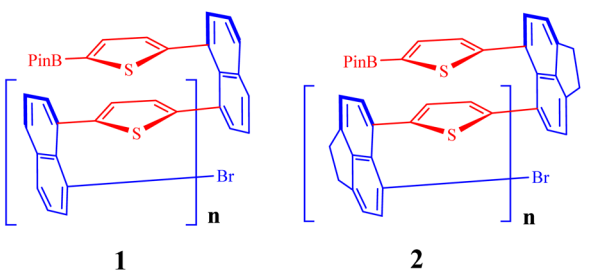

Fig. 1 Synthesized polymers **1** and **2**.

Open Access Article. Published on 23 January 2025. Downloaded on 2/12/2026 10:28:10 AM.
This article is licensed under a Creative Commons Attribution-NonCommercial 3.0 Unported Licence.

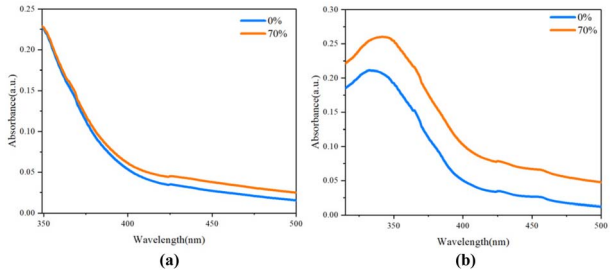

Fig. 2 (a) Ultraviolet (UV) spectroscopy of polymers **1** in different water fractions. (b) Ultraviolet (UV) spectroscopy of polymers **2** in different water fractions (0.05 mg mL^{-1} in THF or THF/H_2O mixture).

observed tailing phenomenon is a critical indicator of the underlying aggregation dynamics within these complex polymer systems.

3.2 Photoluminescence

In contrast to previous studies on the aggregation-induced emission (AIE) of multilayered 3D polymers, our investigation explored fluorescence emission across multiple excitation wavelengths. As illustrated in Fig. 3, the fluorescence emission of polymer **1** was analyzed when excited by wavelengths ranging from 280 nm to 427 nm (Fig. 1(a)). The highest emission intensity was observed at an excitation wavelength of 340 nm, while the lowest intensity occurred at 280 nm. Beyond 340 nm, the emission intensity decreased relative to the maximum observed. Despite the variation in excitation wavelengths, the decline in emission intensity exhibited minimal fluctuation, and the spectral shape remained consistent.

Additionally, changes in chromaticity were reflected in the CIE 1931 coordinates, corresponding to the variations in spectral shape and position (Fig. S1a†), the CIE 1931 coordinates for wavelengths excited at 280 nm, 420 nm, and 427 nm were (0.20168, 0.17485), (0.18135, 0.21635), and (0.19251, 0.31954), respectively. The substantial shifts in chromaticity across these excitation wavelengths suggest a pronounced sensitivity of the polymer's optical properties to the excitation source. Such behavior could be attributed to the unique electronic structure and chiral arrangement of the thiophene-based polymers, which can facilitate distinct electronic transitions and energy transfer mechanisms. The observed coordinate indicates a specific color perception, likely associated with the absorption characteristics of the polymer, which could be engaging in π–π* transitions. As we transition to the longer wavelengths of

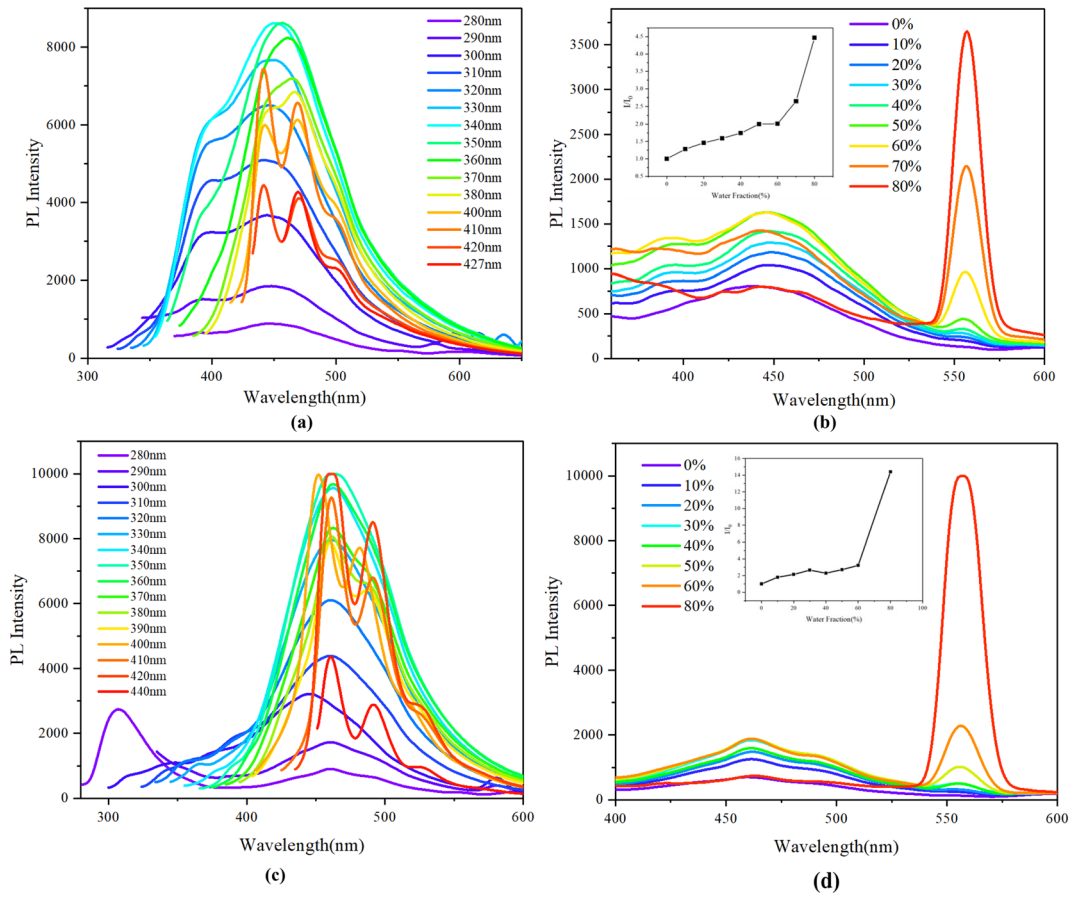

Fig. 3 (a) PL spectroscopy of polymer **1** excited in different wavelengths. (b) PL spectroscopy of polymer **1** excited in 280 nm in different water fractions. (c) PL spectroscopy of polymer **2** excited in different wavelengths. (d) PL spectroscopy of polymer **2** excited in 280 nm in different water fractions.

© 2025 The Author(s). Published by the Royal Society of Chemistry

Open Access Article. Published on 23 January 2025. Downloaded on 2/12/2026 10:28:10 AM.
This article is licensed under a Creative Commons Attribution-NonCommercial 3.0 Unported Licence.

420 nm and 427 nm, the changes in chromaticity coordinates reflect alterations in the excitation dynamics, possibly due to the influence of intermolecular interactions, aggregation states, or conformational changes within the polymer matrix.

In contrast to prior AIE investigations that utilized a single excitation wavelength for emission intensity measurements—typically the highest wavelength in the excitation spectrum. To identify any potential aggregation-induced phenomenon, we use the corresponding lower wavelength as the excited wavelength. The AIE phenomenon is clearly expressed at 450 and 550 nm at the excitation of 280 nm (Fig. 3(b)), with the range of about 550 nm being significantly more observable than the range of 550 nm. Compared to Fig. 3(b), the chroma transfer represented by CIE 1931 coordinates is far more noticeable (Fig. S1b†). The coordinates at water fractions of 0%, 60%, 70%, and 80%, respectively, are (0.1779, 0.15411), (0.18788, 0.19628), (0.21862, 0.26616), and (0.27347, 0.39755). The chroma transfer that takes place is from dark blue to light green. Through this characterization procedure, not only is the aggregate-induced emission phenomena obtained, but also the new regulation of luminescence is realized. We have never seen the luminescence chrominance regulation by aggregate-induced behaviors. We investigated the fluorescence emission phenomenon for polymer **2** adopting the same strategies as polymer **1**. Different excitation wavelengths between 280 and 440 nm are applied to determine the state of emission (Fig. 3(c)). This is significantly different from polymer **1**, where an excitation wavelength of 280 nm causes a large wave to appear between 290 and 350 nm, and where the excitation wavelength is between 300 and 380 nm, the waveform is generally similar, even though their intensities are different (Fig. 3(d)). Whenever the excitation wavelength is greater than 380 nm, the waveform shows a double peak around 460 and 490 nm. The CIE 1931 coordinates for wavelengths excited at 280 nm, 300 nm, and 400 nm were (0.1993, 0.19516), (0.17302, 0.14159), and (0.15388, 0.23835), respectively (Fig. S1c†).

This intriguing phenomenon of chroma transfer in CIE 1931 coordinates is also present in polymer **2** (Fig. S1†), therefore it cannot be a coincidence. The chromaticity coordinates at 280 nm, 300 nm, and 400 nm for CIE 1931 coordinate values are displayed, and their distribution resembles a triangular tendency, in contrast to polymer **1**, which shows a curve-like trend (Fig. S1c†). Furthermore, aggregation-induced emission (AIE) occurs at the excitation wavelength of 280 nm; when the water fraction increases, the emission's intensity increases (Fig. S1d†). Polymer **2**'s AIE phenomenon and polymer **1**'s are comparable (Fig. S1b and c†). The imperfect component is the declining tendency between the 30% and 50% water percentage because of an unfavorable continued rising tendency. However, compared to polymer **1**, the increasing trend is more noticeable for water fractions up to 90% (Fig. 3(d)). The coordinates at water fractions of 0%, 60%, and 80%, respectively, are (0.194170, 0.19041), (0.20587, 0.27030), and (0.31855, 0.53084). The chroma transfer that takes place is from dark blue to light green (Fig. S1d†).

In our investigation of thiophene-based multilayered 3D polymers, we observed a pronounced aggregation-induced emission (AIE) phenomenon when excited at a lower wavelength of 280 nm, contrasting sharply with the lack of AIE at a higher excitation wavelength of 355 nm. This intriguing behavior can be elucidated through the interplay of molecular interactions and the electronic properties of the polymer system.

At the lower excitation wavelength of 280 nm, the energy input is sufficient to promote electronic transitions that favor the formation of excimers or other aggregated species. The close proximity of the polymer chains facilitates non-radiative energy transfer processes, which are characteristic of AIE-active materials. The aggregation allows for a restriction of intramolecular motion, thus enhancing the radiative decay pathways and resulting in a significant increase in emission intensity.

Conversely, at the higher excitation wavelength of 355 nm, the energy could not effectively promote the same excitonic states or aggregate formations that are conducive to AIE. Instead, the excitation could lead to a different set of electronic transitions that do not favor the aggregation-induced enhancement of luminescence. Additionally, the increased energy might induce non-radiative decay processes or promote dissociation of the aggregated species, further diminishing the observable emission.

This differential behavior underscores the critical role of excitation wavelength in modulating the photophysical properties of thiophene-based polymers. It highlights the importance of optimizing excitation conditions to harness the AIE phenomenon effectively, which could have significant implications for the design of advanced luminescent materials in optoelectronic applications. Further investigations into the mechanistic underpinnings of this wavelength-dependent behavior will be essential for developing a comprehensive understanding of AIE in these complex polymer systems.

This differential behavior underscores the critical role of excitation wavelength in modulating the photophysical properties of thiophene-based polymers. It highlights the importance of optimizing excitation conditions to harness the AIE phenomenon effectively, which could have significant implications for the design of advanced luminescent materials in optoelectronic applications. Further investigations into the mechanistic underpinnings of this wavelength-dependent behavior will be essential for developing a comprehensive understanding of AIE in these complex polymer systems.

3.3 Detection of metal ions

Metal ions play crucial roles in various biological and environmental processes; however, their excessive presence can lead to toxicity and environmental degradation. Therefore, the ability to selectively detect and quantify specific metal ions is of paramount importance for both environmental monitoring and biomedical applications. The incorporation of thiophene units into the polymer matrix enhances the selectivity and sensitivity of the sensor. The unique electronic properties of thiophene facilitate strong interactions with target metal ions, allowing for precise detection even at low concentrations. This selectivity is critical in complex matrices where multiple ions could be present.

Open Access Article. Published on 23 January 2025. Downloaded on 2/12/2026 10:28:10 AM.
This article is licensed under a Creative Commons Attribution-NonCommercial 3.0 Unported Licence.

The photoluminescence intensity reflects varying changes in intensity when we add different ionic solutions for polymer **1**. The photoluminescence intensity is approximately between 2000 and 2500 when the specified ionic solution is added, with the majority of the ionic solution showing no significant change. However, it is pretty sensitive to ions of Cr^{6+} and Fe^{3+} (Fig. 4(a) and (b)). With the exception of Cr^{6+} and Fe^{3+}, which are evidently more sensitive than a blank sample devoid of metal ions based on photoluminescence intensity, most metal ions exhibit no discernible sensitivity (Fig. 4(a) and (b)). We also investigated the fluorescence quench ratios according to the increasing concentration of Cr^{6+} and Fe^{3+} ions (Fig. S2a and b†). The multilayered polymer **1** exhibits good sensitivity for Cr^{6+}, and the fluorescence intensity is nearly quenched to the bottom when the concentration of Cr^{6+} ion is up to or greater than 5 μM (Fig. S2a†). Despite the Fe^{3+} ion's sensitivity also having a good reflection, it is not as good as the Cr^{6+} ion in the analyzed circumstance. When the concentration of Fe^{3+} ions reaches or beyond 15 μM, the fluorescence intensity almost completely declines (Fig. S2b†), this situation is not perfect but acceptable for ion detection. The sensitivity of polymer **2** to various metal ions was investigated as well. Similar circumstances applied to polymer **1**, which was able to identify Fe^{3+} and Cr^{6+} ions. Meanwhile, for other metal ions, there is no discernible variation in the fluorescence intensity (Fig. S2c and d†). The multilayered polymer **1** shows excellent sensitivity to Cr^{6+}, and when the concentration of Cr^{6+} ion reaches or exceeds 15 μM, the fluorescence intensity is almost quenched to the bottom (Fig. S2c†). The fluorescence intensity nearly entirely decreases when the concentration of Fe^{3+} ions approach or surpasses 15 μM (Fig. S2d†), although not ideal, this condition is suitable for ion detection.

In this part, thiophene-based multilayered 3D polymer synthesized demonstrates good detection capabilities for Cr^{6+} and Fe^{3+}. Notably, the structural components of this polymer consist solely of thiophene and naphthalene units, devoid of carbonyl or amine functionalities. The ability of our polymer to selectively detect these metal ions can be attributed to the unique electronic and structural properties conferred by the thiophene and naphthalene moieties. Thiophene units are known for their strong electron-donating characteristics, which can facilitate coordination with metal ions. This interaction is likely enhanced by the π-conjugated nature of the polymer, allowing for effective charge transfer processes upon binding with Cr^{6+} and Fe^{3+}. The absence of carbonyl and amine groups in the polymer structure suggests that the detection mechanism could primarily rely on the intrinsic properties of the thiophene and naphthalene units. For Cr^{6+}, the detection could involve complexation or electron transfer processes, as the polymer can stabilize the reduced form of chromium through its electronic

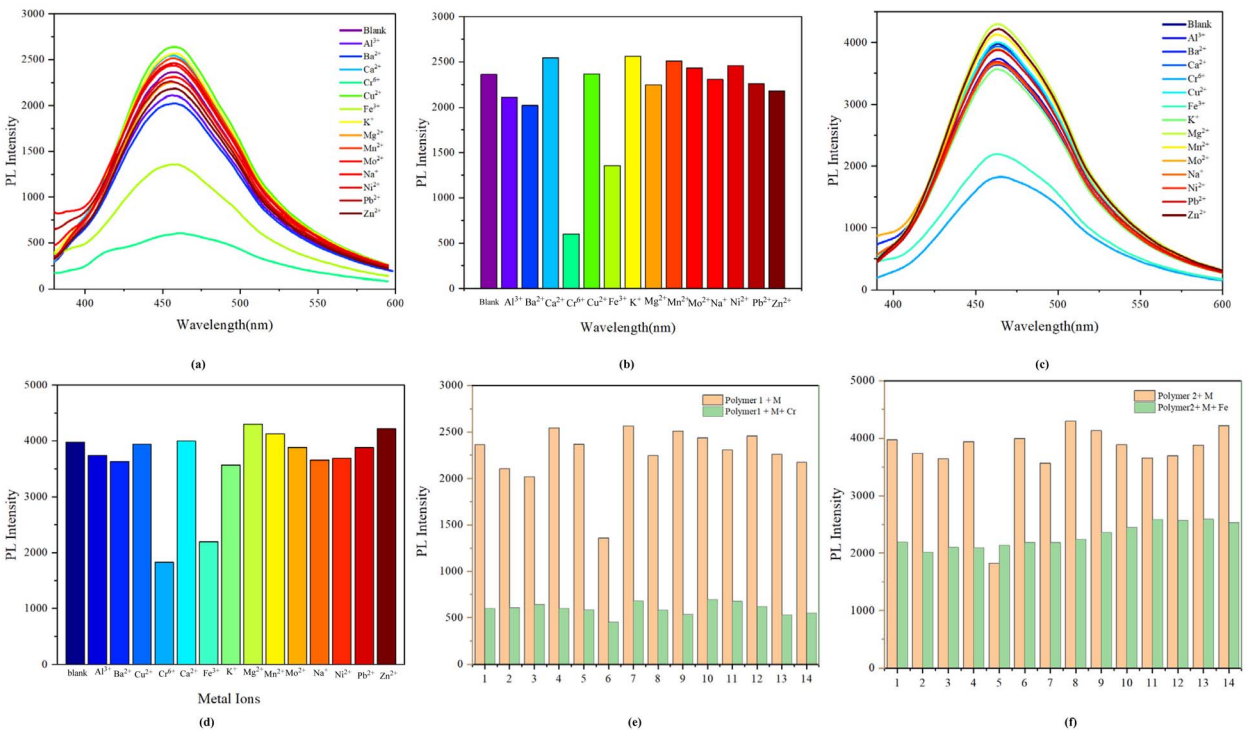

Fig. 4 (a) and (c) PL Spectra of polymers **1** and **2** (0.05 mg mL^{-1}) in the presence of various metals ion solvents of Ba^{2+}, Ca^{2+}, Cr^{6+}, Cu^{2+}, Fe^{3+}, K^{+}, Mg^{2+}, Mn^{2+}, Mo^{2+}, Na^{+}, $Pb^{2+}$and Zn^{2+} 5 μL in PBS buffer (20 mM pH 7.4) solution (THF). Excitation wavelength: 345 nm. (b) and (d) Fluorescence response of 0.05 mg mL^{-1} polymer **1** and **2** to various metal ions. Excitation at 345 nm. (e) PL intensity changes of polymer **1** (0.05 mg mL^{-1}) after adding Cr^{6+} (5 μL) in the presence of various test cations in THF. (1). Blank; (2). Al^{3+}; (3). Ba^{2+}, (4). Ca^{2+}; (5). Cu^{2+}; (6). Fe^{3+}; (7). K^{+}; (8). Mg^{2+}; (9). Mn^{2+}; (10). Mo^{2+}; (11). Na^{+}; (12). Ni^{2+}; (13). Pb^{2+}; (14). Zn^{2+}. (f) PL intensity changes of polymer **2** (0.05 mg mL^{-1}) after adding Fe^{3+} (5 μL) in the presence of various test cations in THF. (1). Blank; (2). Al^{3+}; (3). Ba^{2+}, (4). Ca^{2+}; (5). Cr^{6+}; (6). Cu^{2+}; (7). K^{+}; (8). Mg^{2+}; (9). Mn^{2+}; (10). Mo^{2+}; (11). Na^{+}; (12). Ni^{2+}; (13). Pb^{2+}; (14). Zn^{2+}.

© 2025 The Author(s). Published by the Royal Society of Chemistry

Open Access Article. Published on 23 January 2025. Downloaded on 2/12/2026 10:28:10 AM.
This article is licensed under a Creative Commons Attribution-NonCommercial 3.0 Unported Licence.

structure. Similarly, for Fe^{3+}, the polymer could engage in coordination chemistry, where the thiophene units contribute to the formation of stable complexes with the iron ion. The multilayered architecture of the polymer further enhances its sensitivity and selectivity, as it allows for increased surface area and interaction sites for ion binding. This design not only promotes effective ion capture but also enables the modulation of optical properties, which can be utilized for signal transduction in sensing applications.

The thiophene-based multilayered chiral 3D polymers exhibit promising detection capabilities for Cr^{6+} and Fe^{3+}. Selectivity is a critical requirement for effective sensors, particularly in the presence of competing species. To evaluate the potential of polymer **1** and polymer **2** as ion-selective probes for Cr^{6+} and Fe^{3+} detection, cross-contamination experiments were conducted with these ions coexisting alongside various other metal ions. Polymer **1** demonstrated that the chelating complex formed with Cr^{6+} maintained consistent fluorescence changes even in the presence of other cations. Similarly, polymer **2** exhibited stable fluorescence responses with the chelating complex formed with Fe^{3+} in the presence of competing cations. However, polymer **1** did not show comparable fluorescence changes when complexed with Fe^{3+} in the presence of other cations, and polymer **2** similarly failed to exhibit consistent fluorescence responses when complexed with Cr^{6+} (Fig. 4).

The observed selectivity of thiophene-based multilayered chiral 3D polymers, polymer **1** and polymer **2**, for Cr^{6+} and Fe^{3+} can be attributed to the unique structural characteristics of their subunits. Polymer **1**, characterized by a thiophene–naphthalene framework, exhibits an extensive π-conjugation system that enhances electronic interactions, facilitating the formation of stable chelating complexes with Cr^{6+}. This structure allows for effective energy transfer and consistent fluorescence modulation, enabling polymer **1** to maintain reliable fluorescence changes despite the presence of competing cations.

In contrast, polymer **2**, which incorporates a thiophene–dihydroacenaphthylene structure, demonstrates stable fluorescence responses when complexed with Fe^{3+}. The steric and electronic properties of the dihydroacenaphthylene moiety favorably interact with Fe^{3+}, resulting in effective chelation. However, polymer **2**'s failure to exhibit consistent fluorescence responses with Cr^{6+} suggests that its structural environment is less conducive to Cr^{6+} complexation.

The inability of polymer **1** to show significant fluorescence changes with Fe^{3+} and polymer **2**'s lack of response to Cr^{6+} further underscores the critical role of subunit architecture in determining ion selectivity and sensor performance, highlighting how molecular design influences interaction dynamics with target metal ions.

3.4 Electrochemical performance

Cyclic voltammetry (CV) is a powerful electrochemical technique that plays a crucial role in characterizing multilayered three-dimensional (3D) polymers. The significance of CV lies in its ability to provide insights into the redox behavior, charge transport mechanisms, and electrochemical stability of these advanced materials. The simultaneous occurrence of oxidation and reduction peaks indicated that these multiple π-assemblies possessed electron donation and acceptance capabilities. Around 2.0 V is the point where the oxidation peak for polymer **1** occurs, and around 1.70 V is where the reduction peak occurs (Fig. 5a). The oxidation and reduction maxima for polymer **2** are positioned at around 1.5 and 1.25 V, respectively (Fig. 5b). The cyclic voltammetry (CV) results for the thiophene-based multilayered 3D polymers reveal distinct electrochemical behaviors for polymer **1** and polymer **2**. The oxidation peak of polymer **1** at approximately 2.0 V indicates a higher energy requirement for electron removal, suggesting stronger electron-donating properties or more stable radical cations. In contrast, the reduction peak at around 1.70 V signifies the polymer's ability to accept

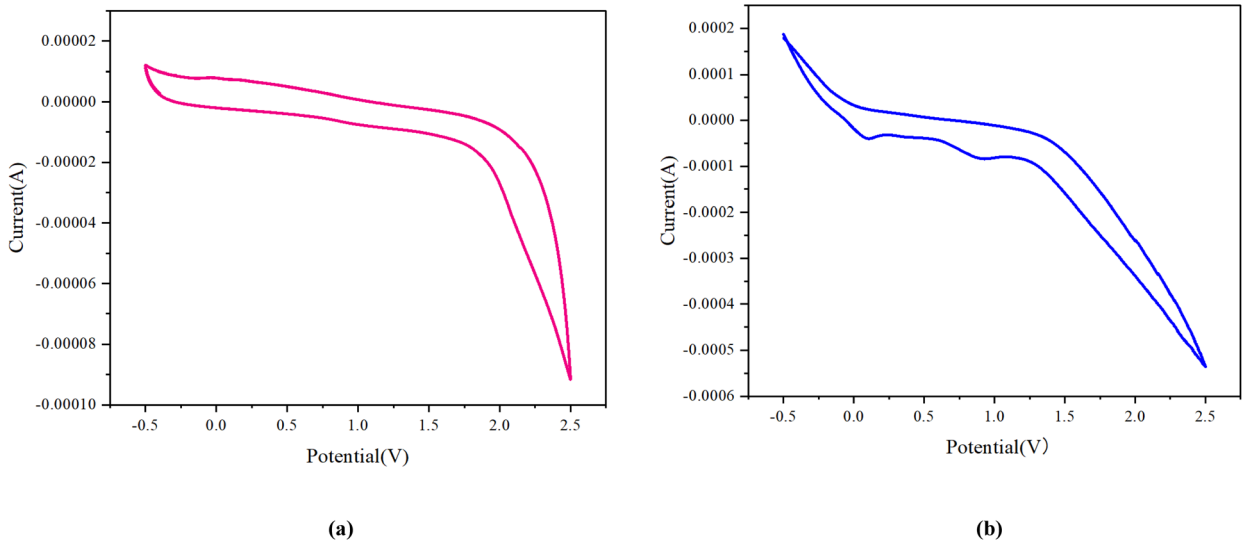

Fig. 5 Electrochemical performance of (a) **1** and (b) **2** in CH_2Cl_2 containing 0.1 M Bu_4NPF_6 as an electrolyte at 298 K; the scan rate is 100 mV s^{-1}.

Open Access Article. Published on 23 January 2025. Downloaded on 2/12/2026 10:28:10 AM. This article is licensed under a Creative Commons Attribution-NonCommercial 3.0 Unported Licence.

electrons, reflecting its electrochemical stability. For polymer **2**, the oxidation and reduction peaks at approximately 1.5 V and 1.25 V, respectively, indicate a lower energy threshold for both oxidation and reduction processes. This suggests that polymer **2** may exhibit enhanced charge transport properties or lower ionization energy compared to polymer **1**.

The distinct electrochemical properties observed in the cyclic voltammetry (CV) results of the thiophene-based multilayered 3D polymers suggest their promising applications in organic electronics. Polymer **1**, with its higher oxidation potential, it could be suitable for use in organic solar cells or transistors, where stability and charge transport are crucial. Conversely, polymer **2**, exhibiting lower oxidation and reduction potentials, could be advantageous for applications in sensors or energy storage devices, where rapid charge transfer is essential. These polymers have the potential to play a variety of functions in cutting-edge electrical and optoelectronic systems, as demonstrated by their distinct electrochemical profiles.

4 Conclusions

In summary, this study has successfully demonstrated the unique properties of the synthesized multilayered 3D polymer, particularly highlighting its aggregation-induced emission (AIE) phenomenon when excited at lower wavelengths, specifically 280 nm. The observed fluorescence enhancement under these conditions underscores the potential of this polymer as a versatile material for optoelectronic applications. Moreover, the multilayered 3D polymer has shown promise as a fluorescence probe for the detection of specific metal ions, indicating its applicability in environmental monitoring and analytical chemistry. The ability to selectively interact with target metal ions while exhibiting distinct fluorescence characteristics positions this polymer as a valuable tool for sensing applications. The electrochemical behaviors of the polymers suggest that they can be potentially applied to electronic devices. Future research will focus on optimizing the multicomponent reaction and functional properties to enhance its sensitivity and selectivity towards a broader range of metal ions. Additionally, further investigations into the underlying mechanisms of the AIE phenomenon and the polymer's interaction with various analytes will contribute to the development of multilayered 3D and oriental chiral molecular materials for sensing and detection technologies.

Data availability

The data that support the findings of this study are available from the corresponding author upon reasonable request.

Author contributions

Sai Zhang: writing – original draft, data curation, methodology, investigation. Qingkai Yuan, Qingzheng Xu and Shenghu Yan: writing – original draft, investigation. Yue Zhang and Guigen Li: project administration and supervision.

Conflicts of interest

The authors declare that they have no known competing financial interests or personal relationships that could have appeared to influence the work reported in this paper.

Acknowledgements

The authors acknowledge the financial support from the Robert A. Welch Foundation (D1361-20210327, USA), National Natural Science Foundation of China (22071102 and 91956110), and National Key Research Plan (2022YFC2105202).

Notes and references

1 H.-J. Li, B.-J. Gui, S.-B. Zhi, H. Wang, S.-C. Han, D. Wang, X.-Y. Wang and J.-H. Yang, *Chin. J. Lumin.*, 2021, **42**, 774–792.
2 A. G. Leal-Junior, C. Marques, H. Lee, K. Nakamura and Y. Mizuno, *Adv. Photonics Res.*, 2022, **3**, 2100210.
3 K. Mazumder, B. Voit and S. Banerjee, *ACS Omega*, 2024, **9**, 6253–6279.
4 Y. Yamamoto, H. Yamagishi, J.-S. Huang and A. Lorke, *Acc. Chem. Res.*, 2023, **56**, 1469–1481.
5 S. G., D. Devadiga, S. B. M. and A. T. N., *J. Fluoresc.*, 2024, DOI: 10.1007/s10895-023-03535-2.
6 Y. Foelen and A. P. H. J. Schenning, *Adv. Sci.*, 2022, **9**, e2200399.
7 Z. Latif, K. Shahid, H. Anwer, R. Shahid, M. Ali, K. H. Lee and M. Alshareef, *Nanoscale*, 2024, **16**, 2265–2288.
8 V. Nocerino, I. Rea, G. Siciliano, L. De Stefano and E. Primiceri, *Trends Anal. Chem.*, 2024, **177**, 117811.
9 G. Wu, Y. Liu, Z. Yang, L. Ma, Y. Tang, X. Zhao, H. Rouh, Q. Zheng, P. Zhou, J.-Y. Wang, F. Siddique, S. Zhang, S. Jin, D. Unruh, A. J. A. Aquino, H. Lischka, K. M. Hutchins and G. Li, *Research*, 2021, **2021**, 3565791.
10 J.-Y. Wang, Y. Tang, G.-Z. Wu, S. Zhang, H. Rouh, S. Jin, T. Xu, Y. Wang, D. Unruh, K. Surowiec, Y. Ma, Y. Li, C. Katz, H. Liang, W. Cong and G. Li, *Chem.–Eur. J.*, 2022, **28**, e202104102.
11 S. Zhang, Q. Yuan and G. Li, *RSC Adv.*, 2024, **14**, 13342–13350.
12 C. Ai, Y. Zhang, S. Zhang and S. Yan, *ChemistrySelect*, 2024, **9**, e202402484.
13 X. Wang, Q. Gao, D. W. Schubert and X. Liu, *Adv. Mater. Technol.*, 2023, **8**, 2300293.
14 Z. Fan, H. Iqbal, J. Ni, N. U. Khan, S. Irshad, A. Razzaq, M. Y. Alfaifi, S. E. I. Elbehairi, A. A. Shati, J. Zhou and H. Cheng, *Int. J. Pharm.: X*, 2024, **7**, 100238.
15 Z. Fan, Z. Ji, F. Zhang, P. Luo, H. Zhang, J. Zhou, H. Cheng and Y. Ding, *Biomater. Sci.*, 2022, **10**, 4889–4901.
16 Z. Fan, Y. Chen, Q. Li, K. Gadora, Z. Ji, D. Wu, J. Zhou, Y. Ding and H. Cheng, *J. Nanopart. Res.*, 2024, **26**, 125.
17 S. P. Rajan, J. Keloth Paduvilan, P. Velayudhan, S. Krishnageham Sidharthan, S. M. Simon and S. Thomas, *J. Polym. Res.*, 2024, **31**, 124.
18 W. Zhou, Q. Liang, A. Wu, W. Shu and W. Yu, *J. Appl. Polym. Sci.*, 2023, **140**, e53727.

© 2025 The Author(s). Published by the Royal Society of Chemistry

Open Access Article. Published on 23 January 2025. Downloaded on 2/12/2026 10:28:10 AM.
This article is licensed under a Creative Commons Attribution-NonCommercial 3.0 Unported Licence.

19 J. Luo, Z. Xie, J. W. Y. Lam, L. Cheng, B. Z. Tang, H. Chen, C. Qiu, H. S. Kwok, X. Zhan, Y. Liu and D. Zhu, *Chem. Commun.*, 2001, 1740–1741.
20 J. Mei, N. L. C. Leung, R. T. K. Kwok, J. W. Y. Lam and B. Z. Tang, *Chem. Rev.*, 2015, **115**, 11718–11940.
21 H. Wang, Q. Li, P. Alam, H. Bai, V. Bhalla, M. R. Bryce, M. Cao, C. Chen, S. Chen, X. Chen, Y. Chen, Z. Chen, D. Dang, D. Ding, S. Ding, Y. Duo, M. Gao, W. He, X. He, X. Hong, Y. Hong, J.-J. Hu, R. Hu, X. Huang, T. D. James, X. Jiang, G.-I. Konishi, R. T. K. Kwok, J. W. Y. Lam, C. Li, H. Li, K. Li, N. Li, W.-J. Li, Y. Li, X.-J. Liang, Y. Liang, B. Liu, G. Liu, X. Liu, X. Lou, X.-Y. Lou, L. Luo, P. R. McGonigal, Z.-W. Mao, G. Niu, T. C. Owyong, A. Pucci, J. Qian, A. Qin, Z. Qiu, A. L. Rogach, B. Situ, K. Tanaka, Y. Tang, B. Wang, D. Wang, J. Wang, W. Wang, W.-X. Wang, W.-J. Wang, X. Wang, Y.-F. Wang, S. Wu, Y. Wu, Y. Xiong, R. Xu, C. Yan, S. Yan, H.-B. Yang, L.-L. Yang, M. Yang, Y.-W. Yang, J. Yoon, S.-Q. Zang, J. Zhang, P. Zhang, T. Zhang, X. Zhang, X. Zhang, N. Zhao, Z. Zhao, J. Zheng, L. Zheng, Z. Zheng, M.-Q. Zhu, W.-H. Zhu, H. Zou and B. Z. Tang, *ACS Nano*, 2023, **17**, 14347–14405.
22 Z. Sheng, Y. Li, D. Hu, T. Min, D. Gao, J.-S. Ni, P. Zhang, Y. Wang, X. Liu, K. Li, H. Zheng and B. Z. Tang, *Research*, 2020, **2020**, 4074593.
23 G. Niu, R. Zhang, X. Shi, H. Park, S. Xie, R. T. K. Kwok, J. W. Y. Lam and B. Z. Tang, *Trends Anal. Chem.*, 2020, **123**, 115769.
24 H. Liu, L.-H. Xiong, R. T. K. Kwok, X. He, J. W. Y. Lam and B. Z. Tang, *Adv. Opt. Mater.*, 2020, **8**, 2000162.
25 X. Cai and B. Liu, *Angew Chem. Int. Ed. Engl.*, 2020, **59**, 9868–9886.
26 F.-Y. Ye, M. Hu and Y.-S. Zheng, *Coord. Chem. Rev.*, 2023, **493**, 215328.
27 A. Gupta, *ChemistrySelect*, 2019, **4**, 12848–12860.
28 X. Wang, C. Shen, C. Zhou, Y. Bu and X. Yan, *Chem. Eng. J.*, 2021, **417**, 129125.
29 G. Wu, Y. Liu, Z. Yang, N. Katakam, H. Rouh, S. Ahmed, D. Unruh, K. Surowiec and G. Li, *Research*, 2019, **2019**, 6717104.
30 G. Wu, Y. Liu, H. Rouh, L. Ma, Y. Tang, S. Zhang, P. Zhou, J.-Y. Wang, S. Jin, D. Unruh, K. Surowiec, Y. Ma and G. Li, *Chemistry*, 2021, **27**, 8013–8020.
31 G. Wu, Y. Liu, Z. Yang, T. Jiang, N. Katakam, H. Rouh, L. Ma, Y. Tang, S. Ahmed, A. U. Rahman, H. Huang, D. Unruh and G. Li, *Natl. Sci. Rev.*, 2020, **7**, 588–599.
32 J. Zhang and L. Kürti, *Natl. Sci. Rev.*, 2021, **8**, nwaa205.
33 Y. Tang, G. Wu, S. Jin, Y. Liu, L. Ma, S. Zhang, H. Rouh, A. I. M. Ali, J.-Y. Wang, T. Xu, D. Unruh, K. Surowiec and G. Li, *J. Org. Chem.*, 2022, **87**, 5976–5986.
34 Y. Liu, G. Wu, Z. Yang, H. Rouh, N. Katakam, S. Ahmed, D. Unruh, Z. Cui, H. Lischka and G. Li, *Sci. China Chem.*, 2020, **63**, 692–698.
35 S. Jin, Y. Wang, Y. Tang, J.-Y. Wang, T. Xu, J. Pan, S. Zhang, Q. Yuan, A. U. Rahman, J. D. McDonald, G.-Q. Wang, S. Li and G. Li, *Research*, 2022, **2022**, 0012.

© 2025 The Author(s). Published by the Royal Society of Chemistry